Theory of the Saffman-Taylor "finger" pattern. I

David A. Kessler
Department of Physics, Rutgers University, Piscataway, New Jersey 08854

Herbert Levine
Schlumberger-Doll Research, Old Quarry Road, Ridgefield, Connecticut 06877-4108

(Received 5 September 1985)

In a series of two papers, we present a comprehensive approach to the pattern formed via viscous "fingering" in a Hele Shaw cell, the Saffman-Taylor finger pattern. We explain how the "finger" width is selected and why this selection cannot be computed via asymptotic analysis in the (large) capillary number. Also, we derive the spectrum of small oscillations around the steady-state shape and show that the selected shape is stable. In this paper, we set up the mathematical and numerical formalism, and demonstrate stability for the $\lambda=\frac{1}{2}$ solution. We also consider the effects of noise on the stability analysis.

I. INTRODUCTION

The problem of the Saffman-Taylor "finger" in a Hele Shaw cell has recently been the subject of renewed interest.[1-3] A Hele Shaw cell[4] is a pair of parallel glass plates separated by a narrow gap. Fluid flow between the plates can be approximated by the two-dimensional Darcy equation $\mathbf{v}=-b^2\nabla p/12\mu$, for gap b and viscosity μ. Much of the interest in this system is due to the similarity of this flow with flow in porous media such as reservoir rock, where a similar relationship holds between pressure and velocity.[5]

If we attempt to displace a fluid in a Hele Shaw cell by a second, *less* viscous fluid, there is an instability[6] which prevents a planar interface from occurring. For a wide range of system parameters, the interface between the two fluids eventually settles down to a single finger with a well-defined shape and velocity.[7,8] This pattern is referred to as the Saffman-Taylor finger pattern. The selection of this pattern and its subsequent breakdown[9] at large flow rate to a more disordered state are characteristic issues that occur in all systems of diffusively controlled pattern formation.

Let us briefly review what is known to date. Using the above two-dimensional approximation to the flow, the equations describing this system can be written as

$$\nabla^2 p = 0 ,$$

$$p(x(s)) = -\gamma\kappa(s) ,$$

$$-\hat{\mathbf{n}}\cdot\frac{d\mathbf{x}(s)}{dt} = \frac{\partial p}{\partial \hat{\mathbf{n}}} ,$$

where the interface is given by $\mathbf{x}(s)$, with normal vector $\hat{\mathbf{n}}$ and curvature κ. The pressure p obeys the further boundary condition $\partial p/\partial y = 0$ at $y=\pm 1$, $p\sim -x$ as $x\to\infty$. With our scaling, the dimensionless parameter γ is given by $(\sigma/12\mu v)(b/a)^2$ where μ is the fluid viscosity, σ the interfacial tension, v the imposed flow at infinity, b the gap thickness, and $2a$ the channel width. Also, we have assumed that the driving fluid has zero viscosity, a situation most closely encountered by displacing with air.

We should note that these equations only approximately describe the actual experiments. There are obviously corrections coming from the three-dimensional nature of the true flow as well as corrections to the simple "microscopic" condition for the pressure drop in terms of surface tension. One might guess, for example, that in analogy with the problem of solidification, there could be an additional pressure drop proportional to the interfacial velocity. Our purpose in studying the simplest set of equations is to derive the essential mechanisms and methodology without aiming at immediate perfect agreement with all aspects of the experiments. As our conclusions unfold, we hope that the reader will agree with us that the inclusion of these other effects will make only small quantitative changes.

Saffman and Taylor showed that in the limit of zero surface tension, the above equations could be solved exactly for steady-state flows. They found a continuous family of possible shapes, labeled by the ratio of "finger" width to channel width, λ. Experimentally, one value of λ is seen for fixed γ. This situation is completely analogous to what occurs in dendritic crystal growth.[10,11] There, in the absence of surface tension, there exists a family of allowed shapes found by Ivantsov,[12] whereas experimentally[13] a unique pattern is found.

The selection of specific values of λ was studied numerically by McLean and Saffman.[14] They showed that if one solved the steady-state problem with nonzero γ, solutions did not exist for arbitrary width λ; also, they found one λ for which a solution did indeed exist. Subsequent work[15] demonstrated that in fact a discrete set (possibly infinite) of λ's could occur. The actual selected pattern does appear to agree[16] with the original solution which corresponds to the smallest possible λ at fixed γ. We denote this as $\lambda^*(\gamma)$. At the same time, McLean and Saffman also attempted to derive the selection principle via an asymptotic expansion in γ, but did not succeed. That is, there seems to exist a well-behaved asymptotic ex-

pansion for the shape for all values of λ. Furthermore, they tried to show that the finger was stable with respect to small perturbations, but concluded that it in fact was unstable. This last result is in manifest contradiction to both the experiments and to computer simulations of Eq. (1).[16]

The purpose of this series of two papers is to provide resolutions to the above-mentioned difficulties. First, we present a new stability analysis which demonstrates that the Saffman-Taylor solution is stable. The numerical demonstration works for small enough velocity, but we will argue that stability is destroyed only at $\gamma=0$ exactly. Some of these results have been presented elsewhere[1] and have been derived independently by Bensimon.[2] The basic idea of our approach is to study the stability operator calculated via an asymptotic expansion in γ.[17] For a wide range of γ, this operator has a spectrum that can be studied numerically with good accuracy. At very small γ ($\lesssim 5\times 10^{-4}$), our numerical techniques become too difficult to implement and we cannot predict what occurs. We will discuss at the end what we feel is the most likely scenario.

At first (in paper I), we restrict the analysis to $\lambda=\frac{1}{2}$. This is the actual selected pattern (λ^*), only in the $\gamma\to 0$ limit. The purpose of this is that we wish to demonstrate the structure of the linear stability operator in the simplest possible case. In particular, we will show the existence of a continuum branch which is always stable as well as the emergence of discrete modes at small γ. The results at $\lambda=\frac{1}{2}$ allow us to explain why an expansion of the eigenfunctions in a small number of Fourier modes is not sufficiently accurate to derive the spectrum, explaining the result of McLean and Saffman.

In the second paper (II), we turn to other values of λ using a similar operator. The most important idea we present is that the selection mechanism is due to an exponentially small term, *invisible* in any standard asymptotic matching analysis. This mechanism causes the breakdown of the connection between the asymptotic expansion and a true steady-state solution. It is only at the discrete set of allowed λ that this connection is restored. This notion allows us to compute the allowed λ via a simple stability criterion, with the results in excellent agreement with the standard approach of Refs. 14 and 15.

Finally, we show that whereas the solution corresponding to $\lambda^*(\gamma)$ is stable, the other members of the discrete set are *always* unstable. This follows immediately from the way in which the stability analysis changes as we increase λ at fixed γ. The result also explains how the spectrum continuously changes from the $\gamma\neq 0$ results discussed here to the $\gamma=0$ spectrum computed by Saffman and Taylor.[6]

As mentioned above, the Saffman-Taylor finger is perhaps the simplest example of pattern formation via interface evolution in a diffusion-controlled system. (Note that we think of the Laplace operator as the quasistatic limit of a diffusion operator.) The mechanisms at work here bear a remarkable resemblance to those which have been shown to apply to simple models of dendritic growth.[11] This leads us to conjecture that this entire class of patterns is determined by including the exponentially small effects of the microscopic parameters, which give rise to global integrability conditions. We have referred to this idea as "microscopic solvability."[18] At the conclusion, we will discuss future directions for research based on this concept.

II. STEADY-STATE SHAPE

In this section we discuss the steady-state finger shape, treating surface tension perturbatively. As discussed above, we limit the details of the analysis to $\lambda=\frac{1}{2}$. The fact that the selection of a discrete set of possible widths is totally invisible in perturbation theory means that our calculation will be internally consistent, keeping systematically all terms linear in γ. In the Appendix, we will present the generalization to arbitrary λ, as that will be needed in paper II.

The original Saffman-Taylor solution at $\gamma=0$ can be most easily expressed via the mapping

$$z=\rho+(1/\pi)\ln(1+e^{-\pi\rho}) , \tag{1}$$

where $z=x+iy$ and $\rho=\phi+i\psi$ for velocity potential ϕ and stream function ψ. The finger interface is given parametrically by setting $\phi=0$. Our goal is to correct this shape perturbatively in the presence of small but nonzero surface tension. This has, in fact, already been done by McLean[19] in a totally different parametrization from the one we find most convenient for the subsequent stability analysis. Inasmuch as we need the explicit form of this correction, we will redo the calculation using our formalism.

Let us assume that the new interface is given by the same mapping as above, except that now $\phi=\delta_0(\psi)$. The pressure field can now be expanded as

$$p=-\phi+\sum_n a_n^{(0)}\cos(n\pi\psi)e^{-n\pi\phi}$$

in terms of the coordinates (ϕ,ψ). Imposing the boundary condition at the interface to $O(\gamma)$, we find

$$-\gamma\kappa(\psi)=-\delta_0(\psi)+\sum_n a_n^{(0)}\cos(n\pi\psi) , \tag{2}$$

where the curvature of the *original* interface, $\kappa(\psi)$, is easily calculated to equal $\pi\,|\cos(\pi\psi/2)|$. This equation determines the expansion coefficients $a_n^{(0)}$ in terms of the as yet unknown $\delta_0(\psi)$.

The remaining condition to be imposed is the velocity constraint $-\hat{\mathbf{n}}\cdot(d\mathbf{x}/dt)=\partial p/\partial\hat{\mathbf{n}}$ for normal vector $\hat{\mathbf{n}}$. After some algebraic manipulations, this equation can be rewritten as

$$\frac{\sin(\pi\psi)\delta_0'+\pi\delta_0}{1+\cos(\pi\psi)}=\sum_n n\pi a_n^{(0)}\cos(n\pi\psi) . \tag{3}$$

We proceed by eliminating $a_n^{(0)}$ from the set of equations. We define an operator $T[\alpha(x)]$ which has the effect of changing a Fourier cosine series into a Fourier sine series:

$$T\left[\sum_n a_n^{(0)}\cos(n\pi\psi)\right]=\sum_n a_n^{(0)}\sin(n\pi\psi) . \tag{4a}$$

Sometimes, it is more convenient to use a principal-value

integral representation of T,

$$T[\alpha(\psi)]=\tfrac{1}{2}\mathrm{P}\int_{-1}^{1}d\psi'\cot[\tfrac{1}{2}\pi(\psi-\psi')]\alpha(\psi')\ . \tag{4b}$$

One can verify that (4a) follows from (4b). In terms of T, the shape correction equation can be written as

$$\frac{\sin(\pi\psi)\delta_0'(\psi)+\pi\delta_0(\psi)}{1+\cos(\pi\psi)}=\frac{\partial}{\partial\psi}T[\delta_0(\psi)-\gamma\kappa(\psi)]\ .$$

Integrating this equation, we arrive at the final form

$$\tan(\pi\psi/2)\delta_0=T[\delta_0-\gamma\kappa]\ . \tag{5}$$

We can solve this equation by assuming that δ_0 can be expanded in a cosine series

$$\delta_0=\sum_n b_n\cos(n\pi\psi)\ . \tag{6}$$

Making use of (4a), and requiring that $\delta_0(\psi)$ vanish at $\psi=\pm1$, we derive the equations

$$b_n=\tfrac{1}{2}\gamma(c_n+c_{n-1}),\quad n\geq 2$$

$$b_1-b_0=\tfrac{1}{2}\gamma c_1\ ,$$

where c_n are Fourier coefficients of $\kappa(\psi)$. One can also specify the condition $b_0=0$ by making use of the translation zero mode. Substituting these expressions into (6) leads to the form

$$\delta_0(\psi)=\frac{\pi}{2}\gamma\cos\left[\pi\frac{\psi}{2}\right][1+\cos(\pi\psi)]$$
$$-\frac{\pi\gamma}{2}\sin(\pi\psi)T\left[\cos\left[\frac{\pi\psi}{2}\right]\right]\ .$$

Finally, the last term can be evaluated explicitly by using the integral expression for T, Eq. (4b). The final expression for the shape correction is

$$\delta_0(\psi)=\frac{\pi\gamma}{2}\cos\left[\frac{\pi\psi}{2}\right][1+\cos(\pi\psi)]$$
$$-\gamma\sin(\pi\psi)\cos\left[\frac{\pi\psi}{2}\right]\ln\left[\frac{1+\tan(\pi\psi/4)}{1-\tan(\pi\psi/4)}\right]\ . \tag{7}$$

The appearance of a logarithm in the first-order shape correction has already been commented on by McLean and Saffman. In particular, they argue that higher orders in γ will lead to higher powers of the logarithm, giving rise to a branch point at the side of the finger. Although this complicates the perturbative analysis by requiring, in general, matching between inner and outer solutions, this does not resolve the problems of either width selection or stability. In our numerical procedures to be discussed later, we change variables to the arclength, converting the above logarithm to a simple *integral* power. Because of this, our results will not depend on the existence of this branch point.

In Sec. III we turn to a calculation of the stability operator, correct to $O(\gamma)$. We will keep terms linear in the *time-dependent* perturbation $\delta(\psi,t)$ and up to linear in γ; this includes cross terms of the form $\gamma\delta$ which are crucial for obtaining the correct spectrum.

III. STABILITY OPERATOR—DERIVATION

In Sec. II we have shown how the steady-state solution is characterized by the function $\phi=\delta_0(\psi)$. We now assume that the interface is perturbed away from $\delta_0(\psi)$, that is, $\phi=\delta_0(\psi)+\delta(\psi,t)$. We keep terms linear in δ, up to $O(\gamma)$.

Let us first consider the equation for the pressure at the interface. Keeping all necessary terms leads to the equation

$$-\gamma\kappa^{(1)}[\delta]=-\delta(\psi,t)+\sum_n a_n\cos(n\pi\psi)$$
$$-\sum_n n\pi a_n^{(0)}\cos(n\pi\psi)\delta(\psi,t)$$
$$-\sum_n n\pi a_n\cos(n\pi\psi)\delta_0(\psi)\ , \tag{8}$$

where $a_n^{(0)}$ are the coefficients used in Sec. II in connection with the shape correction. $\kappa^{(1)}[\delta]$ is the linearized curvature operator given by

$$\kappa^{(1)}[\delta]=-2\cos\left[\frac{\pi\psi}{2}\right]\delta''-\pi\sin\left[\frac{\pi\psi}{2}\right]\delta'$$
$$-\frac{\pi^2}{2}\left[\cos\left[\frac{\pi\psi}{2}\right]+\frac{1}{\cos(\pi\psi/2)}\right]\delta\ . \tag{9}$$

At this stage, we have assumed that the perturbation is symmetric around $\psi=0$. We will return later to the antisymmetric case. Note that $a_n^{(0)}$ as well as δ_0 are proportional to γ. This means that this equation can be solved order by order, to yield

$$\sum_n a_n\cos(n\pi\psi)$$
$$=\delta-\gamma\kappa^{(1)}[\delta]+\delta\sum_n n\pi a_n^{(0)}\cos(n\pi\psi)+\delta_0\frac{\partial}{\partial\psi}T[\delta] \tag{10}$$

with the T operator previously defined.

Again, the system of equations is completed by considering the velocity condition, $-\hat{\mathbf{n}}\cdot(dx/dt)=\partial p/\partial n$. First, the left-hand side can be shown to equal

$$[\tfrac{1}{2}\dot{\delta}(1+\pi\delta_0)+\sin(\pi\psi)\delta'+\pi\delta]/[1+\cos(\pi\psi)]\ . \tag{11}$$

The normal derivative is then evaluated explicitly using the series expression for p. The resulting form is

$$\sum_n n\pi a_n\cos(n\pi\psi)(1-n\pi\delta_0)+\sum_n n\pi a_n^{(0)}\cos(n\pi\psi)(-n\pi\delta)$$
$$-\delta_0'\sum_n n\pi a_n\sin(n\pi\psi)-\delta'\sum_n n\pi a_n^{(0)}\sin(n\pi\psi)\ . \tag{12}$$

Substituting for the a_n using Eq. (10), we derive the alternate representation, correct to $O(\gamma)$:

$$\frac{\partial}{\partial\psi}T[\delta-\gamma\kappa^1[\delta]]+\frac{\partial}{\partial\psi}T\left[\delta\sum_n n\pi a_n^{(0)}\cos(n\pi\psi)\right]+\frac{\partial}{\partial\psi}T\left[\delta_0\frac{\partial}{\partial\psi}T[\delta]\right]$$
$$+\delta_0\delta''+\delta_0'\delta'+\delta'\frac{\partial}{\partial\psi}\left[\sum_n a_n^{(0)}\cos(n\pi\psi)\right]+\delta\frac{\partial^2}{\partial\psi^2}\left[\sum_n a_n^{(0)}\cos(n\pi\psi)\right]. \tag{13}$$

The above expression can be simplified in various ways. First, we can recall from Sec. II that

$$\sum_n a_n^{(0)}\cos(n\pi\psi)=\delta_0-\gamma\kappa^{(0)},$$
$$\sum_n a_n^{(0)}\sin(n\pi\psi)\equiv T[\delta_0-\gamma\kappa^{(0)}]=\delta_0\tan(\pi\psi/2).$$

This enables us to rewrite all the terms which contain $a_n^{(0)}$. More importantly, consider the double transform

$$\frac{\partial}{\partial\psi}T\left[\delta_0\frac{\partial}{\partial\psi}T[\delta]\right]=\frac{1}{4}\frac{\partial}{\partial\psi}\int_{-1}^{1}d\psi'\cot\frac{\pi}{2}(\psi-\psi')\delta_0(\psi')\frac{\partial}{\partial\psi'}\int_{-1}^{1}d\psi''\cot\frac{\pi}{2}(\psi'-\psi'')\delta(\psi'')$$
$$=\frac{1}{4\pi^2}\frac{\partial}{\partial\psi}\int_{-\infty}^{\infty}\left[\frac{1}{\psi-\psi'+i\epsilon}+\frac{1}{\psi-\psi'-i\epsilon}\right]\delta_0(\psi')\left[\frac{1}{\psi'-\psi''+i\epsilon}+\frac{1}{\psi'-\psi''-i\epsilon}\right]\delta'(\psi'')d\psi'd\psi''.$$

Using the expansion for δ_0 in Sec. II as $\sum_n b_n\cos(n\pi\psi)$, one can explicitly integrate over ψ' via the residue theorem. The result is

$$\frac{\partial}{\partial\psi}T\left[\delta_0\frac{\partial}{\partial\psi}T[\delta]\right]=-\frac{\partial}{\partial\psi}(\delta_0\delta')+\frac{\partial}{\partial\psi}\int\Lambda(\psi,\psi')\delta'(\psi')$$

with the kernel

$$\Lambda(\psi,\psi')=\tfrac{1}{2}\cot[(\pi/2)(\psi-\psi')][l(\psi)-l(\psi')], \tag{14a}$$
$$l(\psi)=\tan(\pi\psi/2)\delta_0+\gamma T[\kappa^{(0)}]. \tag{14b}$$

Combining all the pieces and using the known expressions for δ_0 and $T[\kappa^{(0)}]$ to simplify $l(\psi)$, we arrive at the stability equation

$$[\tfrac{1}{2}\dot{\delta}(1+\pi\delta_0)+\sin(\pi\psi)\delta'+\pi\delta]/[1+\cos(\pi\psi)]$$
$$=\tfrac{1}{2}\int_{-1}^{1}d\psi'\cot[\tfrac{1}{2}\pi(\psi-\psi')]\left[(\delta-\gamma\kappa^1[\delta])'+\left[\delta(\psi')\frac{\partial}{\partial\psi'}[\delta_0\tan(\tfrac{1}{2}\pi\psi')]\right]'\right.$$
$$\left.+[l'(\psi)-l'(\psi')]\delta'(\psi')+[l(\psi)-l(\psi')]\delta''(\psi')\right]+\frac{\partial}{\partial\psi}[\delta(\delta_0-\gamma\kappa^{(0)})'] \tag{15}$$

with

$$l(\psi)=\frac{\pi}{2}\gamma\sin\left[\frac{\pi\psi}{2}\right][1+\cos(\pi\psi)]+2\gamma\cos\left[\frac{\pi\psi}{2}\right][1+\cos(\pi\psi)]\ln\left[\frac{1+\tan(\pi\psi/4)}{1-\tan(\pi\psi/4)}\right]. \tag{16}$$

A similar type of equation appears in the work of Muller-Krumbhaar and Langer[20] in the context of the dendrite system.

Equation (15) is the basic stability equation for symmetric perturbations. We will turn to a numerical analysis of this operator in Sec. V. Before this, however, we wish to present several analytical results. This includes a derivation of the dispersion relation for the continuum modes as well as an explicit verification of the presence of a translation zero mode. These calculations will be the subject of Sec. IV.

To conclude this section, we now present the analogous formulation for antisymmetric perturbations. The expansion for the pressure analogous to the cosine series used above is

$$P=-\phi+\sum_n\tilde{a}_n\sin[(n+\tfrac{1}{2})\pi\psi]e^{-(n+1/2)\pi\phi}+\sum_n a_n^{(0)}\cos(n\pi\psi)e^{-n\pi\phi}$$

which also satisfies the sidewall conditions, $(\partial p/\partial\psi)\,|_{\psi=\pm1}=0$. The first equation leads to the following expression for the $\tilde{a}_n$:

$$\sum_n\tilde{a}_n\sin[(n+\tfrac{1}{2})\pi\psi]=\delta-\gamma\kappa^1[\delta]+\delta\frac{\partial}{\partial\psi}\sum_n a_n^{(0)}\sin(n\pi\psi)+\delta_0\frac{\partial}{\partial\psi}\tilde{T}(\delta), \tag{17}$$

where the new transform $\tilde{T}$ has the effect

$$\tilde{T}[\sin[(n+\tfrac{1}{2})\pi\psi]]=-\cos[(n+\tfrac{1}{2})\pi\psi]$$

and the explicit representation

$$\tilde{T}[\delta(\psi)]=\tfrac{1}{2}\mathrm{P}\int_{-1}^{1}d\psi'\frac{1}{\sin[\frac{1}{2}\pi(\psi-\psi')]}\delta(\psi') .$$

Substituting this into the velocity equation, we now have the form

$$[\tfrac{1}{2}\dot{\delta}(1+\pi\delta_0)+\sin(\pi\psi)\delta'+\pi\delta]/(1+\cos\pi\psi)$$

$$=\frac{\partial}{\partial\psi}\tilde{T}[\delta-\gamma\kappa^{1}[\delta]]+\frac{\partial}{\partial\psi}\tilde{T}\left[\delta\sum_n n\pi a_n^{(0)}\cos(n\pi\psi)\right]+\frac{\partial}{\partial\psi}\tilde{T}\left[\delta_0\frac{\partial}{\partial\psi}\tilde{T}\right]+(\delta_0\delta')'+\left[\delta\left[\sum_n a_n^{(0)}\cos(n\pi\psi)\right]'\right]' .$$

This is exactly the same result as before, just with T replaced everywhere by $\tilde{T}$. To conclude the calculation, we note that the double transform term

$$\frac{\partial}{\partial\psi}\tilde{T}\left[\delta_0\frac{\partial}{\partial\psi}\tilde{T}(\delta)\right]$$

can be reduced to the single integral of exactly the same form as before, with the only change being the replacement of $\Lambda(\psi,\psi')$ with $\tilde{\Lambda}(\psi,\psi')$:

$$\tilde{\Lambda}(\psi,\psi')=\tfrac{1}{2}\csc[\tfrac{1}{2}\pi(\psi-\psi')][l(\psi)-l(\psi')] .$$

For a single finger, the only possible perturbations consistent with the sidewall conditions are the symmetric and antisymmetric ones. For a multifinger array, we can allow, in general, perturbations that are labeled by a Bloch wave vector k corresponding to how the perturbation on one finger is related to the perturbation of the translated finger. This leads to a new eigenvalue problem, indexed by the label k. This analysis, as well as its implications for the coalescence of finger arrays into a single finger final shape, will be presented elsewhere.[21]

IV. STABILITY OPERATOR—ANALYSIS

In Sec. V we will tackle the numerical evaluation of the spectrum of the operators that we have derived. First, however, we would like to exhibit two analytic computations; these are the demonstration of the existence of a translational zero mode and the derivation of a dispersion relation for the continuum part of the spectrum.

The original finger shape has an obvious invariance with respect to translations along the flow direction. This gives rise to a zero mode in the linear oscillations spectrum. Our approach will be to compute the zero mode explicitly and then verify that it indeed satisfies the eigenvalue equation derived in Sec. III.

Consider making a shift Δ in the x direction of the pattern described by (1). The normal shift is then

$$\hat{\mathbf{n}}\cdot\Delta\mathbf{x}=\hat{\mathbf{n}}_x\Delta .$$

We must equate this to the normal shift induced by a nonzero perturbation $\hat{\delta}$:

$$\hat{\mathbf{n}}_x\Delta=(\hat{\mathbf{n}}_x x_\phi+\hat{\mathbf{n}}_y y_\phi)\hat{\delta} .$$

We now evaluate all these objects around the interface $x(\delta_0(\psi),\psi),y(\delta_0(\psi),\psi)$ and keeps terms to $O(\gamma)$. The result is

$$\hat{\delta}=\Delta[1+\cos(\pi\psi)]-\Delta[\pi\delta_0\cos(\pi\psi)-\delta_0'\sin(\pi\psi)] .$$

The second term is, of course, proportional to the small parameter γ. Recall that the stability operator also could be broken up into terms independent of γ and terms linear in γ: Schematically $L[\delta]=L_0[\delta]+\gamma L_1[\delta]$. Consistency to this order requires that

$$L_0[\delta_0\cos(\pi\psi)-\delta_0'\sin(\pi\psi)]=\gamma L_1[1+\cos(\pi\psi)] . \tag{18}$$

This is the equation we will now check.

Let us go back to the form of the stability operator in (13) and (11). Substituting the above functions, we derive the condition

$$-\tan\left[\frac{\pi\psi}{2}\right][\delta_0\cos(\pi\psi)-\delta_0'\sin(\pi\psi)]+T[\delta_0\cos(\pi\psi)-\delta_0'\sin(\pi\psi)]$$

$$=(\delta_0-\kappa^{(0)})'[1+\cos(\pi\psi)]-\pi\sin(\pi\psi)\delta_0+T[-\gamma\kappa^{(1)}[1+\cos(\pi\psi)]+\delta_0'\sin(\pi\psi)+\delta_0[1+\cos(\pi\psi)]] .$$

From its definition,

$$\kappa^{(1)}[1+\cos(\pi\psi)]=\pi^2\left[\cos^3\left[\frac{\pi\psi}{2}\right]-\cos\left[\frac{\pi\psi}{2}\right]\right] .$$

We rewrite $T[-\delta_0'\sin(\pi\psi)]$ via the equation for δ_0, Eq. (5), as $-[1+\cos(\pi\psi)](\delta_0-\kappa^{(0)})'-\pi T(\delta_0)$. After some algebraic manipulations, we obtain

$$\tan\left[\frac{\pi\psi}{2}\right][\delta_0'\sin(\pi\psi)-\delta_0\cos(\pi\psi)]$$
$$=-\frac{\gamma\pi^2}{2}T\left[[1+\cos(\pi\psi)]\cos\left[\frac{\pi\psi}{2}\right]\right]$$
$$-(\delta_0-\kappa^{(0)})'[1+\cos(\pi\psi)]$$
$$-\pi\sin(\pi\psi)\delta_0-\pi\delta_0\tan\left[\frac{\pi\psi}{2}\right].$$

To make further progress, we use the relationship

$$T[[1+\cos(\pi\psi)]f(\psi)]$$
$$=[1+\cos(\pi\psi)]T[f(\psi)]+\tfrac{1}{2}\sin(\pi\psi)\int_{-1}^{1}d\psi f(\psi)$$

which can be derived from the definition of T. Now,

$$+\frac{\pi^2}{2}T\left[\cos\left[\frac{\pi\psi}{2}\right]\right]=\pi\cos\left[\frac{\pi\psi}{2}\right]\ln\left[\frac{1+\tan(\pi\psi/4)}{1-\tan(\pi\psi/4)}\right]$$

and $\frac{1}{2}\int_{-1}^{1}\cos(\pi\psi/2)d\psi=2/\pi$. Substituting all these results into the above expression and replacing δ_0 by the expression given in Eq. (7), we indeed verify that the above equation is satisfied. The existence of an approximate [to $O(\gamma^2)$] zero mode will serve as a useful check on our numerical computations.

The next thing we wish to discuss is the existence of a continuous spectrum. In the absence of surface tension, all eigenmodes of linear stability operator decay exponentially with distance away from the finger tip. With surface tension, we must in general allow for the possibility of modes which oscillate with finite wave vector, a sort of diffusive capillary wave behavior. Seen in terms of the original parametrization of the interface, these eigenfunctions will have singularities at $\psi=\pi/2$, similar, in fact, to the branch point structure which arises in perturbation theory. To see how all this comes about, we reexpress the stability operator in terms of the physical arclength, related to ψ via the condition

$$\cos\left[\frac{\pi\psi}{2}\right]=\frac{1}{\cosh(\pi s)}.$$

In terms of s, the shape correction becomes

$$\delta_0(s)=\pi\gamma/\cosh^3(\pi s)$$
$$-2\gamma\pi s\tanh(\pi s)/\cosh^2(\pi s). \quad (19)$$

This, as promised previously, is just a power times hyperbolic functions and has no singularities. We can now evaluate the stability operator as follows. The left-hand side of the stability equation reduces to

$$\tfrac{1}{2}\cosh^2(\pi s)[\tfrac{1}{2}\dot{\delta}(1+\pi\delta_0)+\pi\delta+\tanh(\pi s)\delta'], \quad (20a)$$

where derivatives are now taken with respect to s. Similarly, the right-hand side becomes

$$\tfrac{1}{2}\int_{-\infty}^{\infty}ds'\frac{1+\sinh(\pi s)\sinh(\pi s')}{\sinh(\pi s)-\sinh(\pi s')}\left[(\delta-\gamma\tilde{\kappa}^{(1)}[\delta])'+\left[\tfrac{1}{2}\delta\cosh(\pi s')\frac{\partial}{\partial s}[\delta_0\sinh(\pi s')]\right]'\right.$$
$$\left.+\tfrac{1}{2}[\cosh(\pi s)\tilde{l}'(s)-\cosh(\pi s')\tilde{l}'(s')]\delta'+\tfrac{1}{2}[\tilde{l}(s)-\tilde{l}(s')][\cosh(\pi s')\delta']'\right]$$
$$+\tfrac{1}{4}\cosh(\pi s)\{\delta\cosh(\pi s)[\delta_0-\gamma\pi/\cosh(\pi s)]'\}' \quad (20b)$$

with

$$\tilde{\kappa}^{(1)}=-\tfrac{1}{2}\cosh(\pi s)\delta''-\pi\sinh(\pi s)\delta'$$
$$-\tfrac{1}{2}\pi^2\delta\left[\cosh(\pi s)+\frac{1}{\cosh(\pi s)}\right]$$

and

$$\tilde{l}(s)=\pi\gamma\tanh(\pi s)/\cosh^2(\pi s)+2\gamma\pi s/\cosh^3(\pi s).$$

A continuum mode is a solution $\delta\sim e^{\pi k s}$. We can compute a dispersion relationship by keeping only those terms that vary asymptotically as $e^{\pi s(k+2)}$. Because both l and δ_0 decay rapidly as $s\to\pm\infty$, they make no contribution. Note too that $\mathrm{Re}k\leq 0$ for the integral to converge. For k in this range, we find

$$\frac{\omega}{2\pi}=-q-\tfrac{1}{2}\gamma\pi^2q^3\tan\left[\frac{\pi q}{2}\right], \quad (21)$$

$q\equiv k+1$, and hence $\mathrm{Re}q\leq 1$. This, of course, is the same result as one finds without including any shape correction.[1] In this notation, a discrete mode such as the translation zero mode has $\mathrm{Re}k=-2$. For this value of $\mathrm{Re}k$, all of the s' range contributes equally. It is easy to show that $\mathrm{Re}q$ corresponds to the rate of growth of the normal displacement away from the Saffman-Taylor interface.

Finally, we would like to reemphasize the drastic change in the stability operator introduced when γ is taken to be any nonzero value. The cause of this is simply that γ enters with a higher derivative term and hence changes the character of the allowed eigenfunctions. Because of this, eigenfunctions at small γ are not well approximated by linear combinations of a small number of $\gamma=0$ modes, of the type used by McLean and Saffman (see in this regard the discussion in Ref. 19). As we shall soon see, keeping only a small number of modes leads to the erroneous conclusion that fingers are unstable.

V. NUMERICAL PROCEDURE

We have not found any analytical means of fully analyzing the spectrum of the linear stability operator given in Sec. IV. We, therefore, turn to a numerical diagonalization via discretizing the arclength s. This involves the introduction of two cutoff parameters, the number of

points N, and the maximum arclength $s_{\max}$. It will prove more convenient to work with $s_{\max}$ and a spatial cutoff, defined as $\sigma=s_{\max}/N$. The issues that will be discussed in this section include how to discretize the principal-value integral and how to extrapolate our results to the limit ($\sigma\to 0$, $s_{\max}\to\infty$). The operator we wish to study was given in Eqs. (20a) and (20b) in terms of arclength. We let $s_j=j\sigma$, $j=0,N$, and impose either $\delta'(0)=0$ (for symmetric modes) or $\delta(0)=0$ (asymmetric modes). In all cases, $\delta(s\geq s_{\max})=0$. The derivative operators are discretized directly. The integral is rewritten as (Q stands for the entire rest of the integrand)

$$\frac{1}{2}\int_{-\infty}^{\infty} ds' \frac{1+\sinh(\pi s)\sinh(\pi s')}{\sinh(\pi s)-\sinh(\pi s')} Q(s') = \frac{1}{2}\sum_{j=-N}^{N-1} \mathrm{P}\int_{\sigma(j-1/2)}^{\sigma(j+1/2)} ds' \left[\frac{1+\sinh(\pi s)\sinh(\pi s')}{\sinh(\pi s)-\sinh(\pi s')}\right][Q(j\sigma)+Q'(j\sigma)(s'-j\sigma)] .$$

The integrals are then done either analytically or approximately with an error of $O(1/N^2)$. The accuracy of this method (i.e., dropping terms in Q'', etc.) can easily be shown to be $O(1/N^2)$. A similar methodology works for the antisymmetric modes, where the operator now has the kernel $\cosh(\pi s)\cosh(\pi s')/[\sinh(\pi s)-\sinh(\pi s')]$.

We first test the program by looking at the approximate zero mode discussed above. Schematically, the operator under consideration can be written as

$$L[\delta]=L_0[\delta]+\gamma L_1[\delta] ,$$

and we showed earlier that analytically

$$L_0[\delta_0\cos(\pi\psi)-\delta_0'\sin(\pi\psi)]=\gamma L_1[1+\cos(\pi\psi)]$$

for $\delta_0(\psi)$ given in Eq. (19). We can substitute this identity into our program to determine both the code validity and the intrinsic error. In addition, we wrote a separate code for arbitrary λ (which will be used in paper II) and determined that it agreed with the numbers derived here when specialized to $\frac{1}{2}$, as well as the exact results[6] for $\lambda=1$.

We expect that for any given value of γ, there will be both discrete modes and a continuum. For the discrete modes, we expect that the eigenfunctions will decrease exponentially with arclength and that therefore the eigenvalues will be practically independent of $s_{\max}$. On the other hand, we expect convergence at fixed $s_{\max}$ to be quadratic. To verify this behavior, we have done tests at various values of $s_{\max}$ and N. A typical set of data, for $\gamma=0.005$, is contained in Table I. The eigenvalue given there corresponds to the eigenvector plotted in Fig. 1.

There are several important points to notice. At fixed σ, there is practically no change in the eigenvalues as a function of $s_{\max}$. For fixed $s_{\max}$, the points fall exactly (to three significant figures) on a curve of the form

$$E_N=E_\infty+\delta E/N^2,\quad E_\infty=-0.1076 .$$

We can therefore extract the actual eigenvalue by simple extrapolation. Note also that as we lower the number of points, the mode becomes *less* stable. This is an important idea. It accounts, as mentioned above, for the inability of the original stability calculation of McLean and Saffman,[14] which was limited to 15 Fourier modes, to see the stabilization of the finger due to surface tension. Later, we will argue that this effect may also cause the observed width to fall below $\frac{1}{2}$.

TABLE I. Discrete eigenvalue, dependence on N and arclength cutoff.

N \ $s_{\max}$	2	4	6	8
100	−0.0952			
200		−0.0952		
300		−0.1021	−0.0953	
400		−0.1045		−0.0954
450			−0.1021	

Continuum modes correspond either to real eigenvalues with $\mathrm{Re}\omega\ll 0$ or to complex-conjugate eigenvalue pairs. A typical eigenvector of the first type is shown in Fig. 2. Notice that $\mathrm{Im}q$ is quite large whereas $\mathrm{Re}q$ is relatively small (recall that the rate of growth is $\mathrm{Re}k\equiv\mathrm{Re}q-1$). Inasmuch as these modes are always extremely damped, we need not worry about accurate extrapolation.

In Table II we present a sampling of our data at $\gamma=0.001$ for several of the lowest modes corresponding to complex eigenvalues. One such mode is plotted in Fig. 3; now $\mathrm{Im}q$ is small and $\mathrm{Re}\omega$ can be near $\mathrm{Re}\omega=0$. The question of extrapolating to limits $s_{\max}\to\infty$, σ fixed and then $\sigma\to 0$ is thus more critical. This is obviously difficult to do very accurately, given the practical limits on the size of $s_{\max}$. We chose to proceed as follows. Let us consider fixing $j/s_{\max}$ by looking at different modes for different $s_{\max}$:

mode 1: $\equiv j_1=s_{\max}/4$,

mode 2: $\equiv j_2=s_{\max}/2$,

mode k: $\equiv j_k=ks_{\max}/4$.

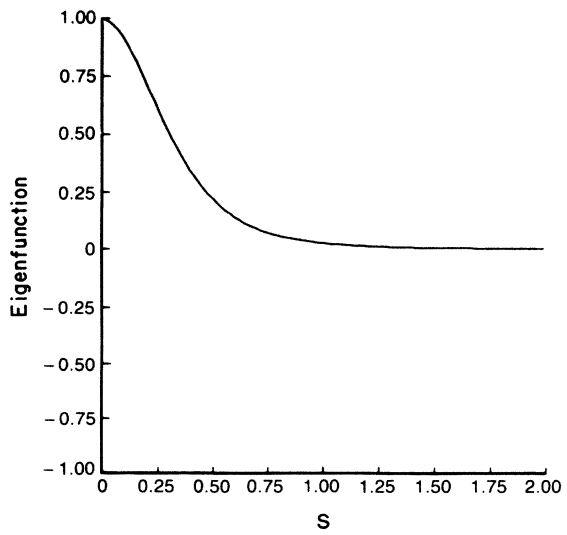

FIG. 1. Symmetric "zero-mode" eigenfunction.

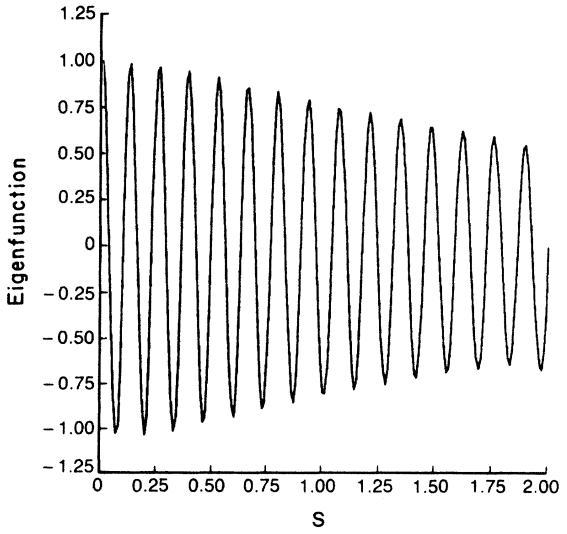

FIG. 2. High-q, real continuum mode.

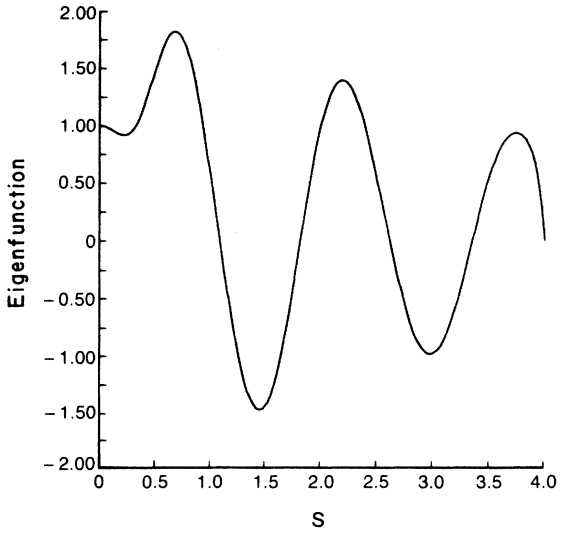

FIG. 3. Small-q, complex continuum mode.

We then construct sequences at a fixed mode number and increasing $s_{\max}$. (If j is fractional at some $s_{\max}$, we interpolate to find the eigenvalue.) This procedure corresponds to fixing the wave vector Imq to be finite and then taking the large-distance limit. We then assume an error of $1/s_{\max}$. For the lowest mode, we also extrapolate the answer to Im$q=0$, which corresponds to the bottom of the continuum. The results of this analysis are tested to be insensitive to the exact form of the mode selection procedure and the interpolation.

The most important features of the continuum eigenvalues to be presented later are (a) they are all negative and (b) our procedure generates an upper bound on Reω. The latter is true because increasing σ always stabilizes and we have made the worst possible assumption about convergence in $s_{\max}$. Even with our inherent inaccuracy, the continuum always turns out to be stable at all γ and λ and hence the actual precise magnitude of the modes will be unimportant. All graphs of the complex continua should be interpreted, though, to be merely an upper bound on Reω.

VI. DISCRETE MODES

A discrete mode is an eigenfunction of the stability operator which decays with Re$q=-1$. These modes all turn out to have Im$q=0$. One such mode should arise

TABLE II. Continuum eigenvalues, dependence on spatial and arclength cutoffs.

100σ \ $s_{\max}$	2	4	6
		(−0.815,0.263)	(−0.598,0.170)
	(−0.972,0.520)	(−0.817,0.639)	(−0.611,0.480)
2	(−1.20,0.922)	(−0.905,0.995)	(−0.644,0.760)
	(−1.54,1.48)	(−1.01,1.37)	(−0.690,1.03)
		(−1.12,1.76)	(−0.795,1.59)
			(−0.853,1.88)
		(−0.840,0.275)	
$\frac{4}{3}$	(−0.968,0.537)	(−0.835,0.649)	(−0.615,0.173)
	(−1.19,0.957)	(−0.921,1.00)	(−0.625,0.485)
	(−1.52,1.52)	(−1.02,1.39)	(−0.655,0.766)
		(−1.14,1.78)	(−0.700,1.04)
			(−0.749,1.32)
			(−0.801,1.60)
	(−0.965,0.543)	(−0.856,0.283)	
1	(−1.19,0.971)	(−0.847,0.652)	
	(−1.52,1.54)	(−0.933,1.01)	
		(−1.04,1.39)	
		(−1.14,1.78)	

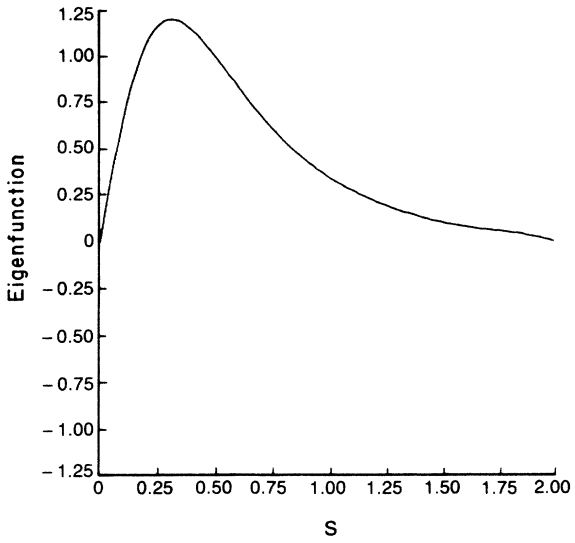

FIG. 4. Antisymmetric discrete eigenfunction.

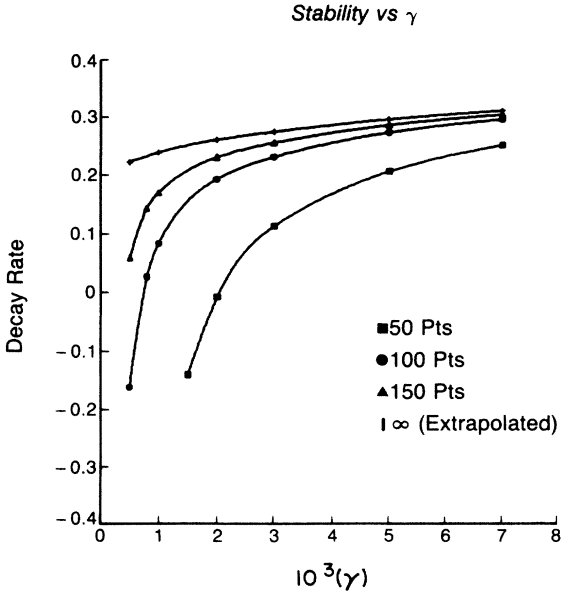

FIG. 5. Antisymmetric eigenvalue, as a function of γ, at different values of N.

from the existence of translation invariance. That is, there should be a zero mode, $\mathrm{Re}\omega=0$, which is symmetric around $\psi=0$. In addition, there might be other modes both symmetric and antisymmetric which can be identified numerically.

Let us first consider the translation mode. As discussed earlier (Sec. IV), the stability operator is of the form $L=L_0+\gamma L_1$ where there exists a function $\delta_0(\psi)$ such that $\delta_0(\psi)=\delta_0^0(\psi)+\gamma\delta_0^1(\psi)$, with $L_0[\delta_0^0]=0$, $L_1[\delta_0^0]+L_0[\delta_0^1]=0$. This analytic result does not require that there be an exact zero mode in the spectrum of L. In fact, we know already that the spectrum of L cannot be derived perturbatively because γL_1 drastically alters the nature of the stability operator. However, there still should be an approximate zero mode because of the following reasoning. At small γ, the exact solution of the steady-state problem approaches the $\lambda=\frac{1}{2}$ Saffman-Taylor solution.[14] The exact stability operator has a zero mode because of translation invariance and the operator here is in some sense "close" to that operator. We therefore expect to find a discrete mode close to $\mathrm{Re}\omega=0$.

We have runs at $\gamma=0.007$, 0.005, 0.003, 0.002, and 0.001 and performed the extrapolations discussed above. The result is that there is one discrete symmetric mode which in all cases is close to $\mathrm{Re}\omega=0$. The results are given in the following table.

γ	0.007	0.005	0.003	0.002	0.001
ω_0	−0.099	−0.108	−0.117	−0.123	−0.135

All the values are negative, a result that will be important for the ideas to be presented in paper II. Somewhat surprisingly, ω_0 becomes larger as γ gets smaller. For all $\gamma\geq 0.003$, there are no additional symmetric discrete modes. For γ below this, there appear to be additional modes, the lowest one at $\mathrm{Re}\omega\sim -9$ at $\gamma=0.001$. These modes "break off" from the bottom of the real continuum—as we go to smaller γ, more and more of them can occur. This is presumably connected to the decrease of $\mathrm{Re}\omega$ at which the continuum stops, derived in Sec. VII. For our purposes here, these modes remain extremely damped, and we need not worry about their exact values.

We now turn to antisymmetric modes at similar values of γ. There is now no general reason for the occurrence of any specific eigenvalue, and we rely completely on our numerical procedure. The results for the lowest mode are presented below and a graph of the eigenfunction is shown in Fig. 4.

γ	0.007	0.005	0.003	0.002	0.001	8×10^{-4}	5×10^{-4}
$\tilde{\omega}_0$	−0.313	−0.298	−0.277	−0.262	−0.241	−0.236	−0.223

Unlike ω_0, $\tilde{\omega}_0$ gets smaller as $\gamma\to 0$. We see no indications that it actually crosses zero before $\gamma=0$, although we cannot go much below 5×10^{-4}.

Bensimon[2] has suggested that noise plays an important role in the antisymmetric instability observed to occur in experiments at small enough γ. To check this idea, we can interpret the finite number of points in the numerical algorithm as a simple way to mimic the effects of imperfections in the experiments. In Fig. 5, we have graphed the convergence of $\tilde{\omega}_0$ as a function of N to its asymptotic value. We have found the following behavior.

(a) At any fixed N, there exists a value of $\gamma=\gamma^*$ at which the antisymmetric mode becomes unstable. As $N\to\infty$, $\gamma^*\to 0$.

(b) The number of points needed to stabilize a fixed γ increases rapidly as $\gamma\to 0$.

Thus, we agree that even if there is strictly a transition without noise only at $\gamma=0$, finite noise might give rise to an antisymmetric instability at finite γ. We will have more to say about the effects of noise in paper II when we generalize our treatment to arbitrary λ.

VII. CONTINUUM MODES

We now present our results regarding the continuous part of the spectrum. As mentioned earlier, there are both real and complex branches of eigenvalues. Let us first focus on the real part. In Sec. IV we derived the dispersion relation

$$\omega=-q-\tfrac{1}{2}\gamma\pi^2q^3\tan(\pi q/2)\ .$$

To ensure convergence, $\mathrm{Re}q\le 1$, and a real spectrum requires for large $\mathrm{Im}q$

$$\mathrm{Im}q=\tfrac{3}{2}\gamma\pi^2\mathrm{Re}q(\mathrm{Im}q)^2$$

or $\mathrm{Re}q\ge 0$. Therefore, the real spectrum extends from $\omega=-\infty$ at $\mathrm{Re}q=0$, $\mathrm{Im}q=\infty$ to a finite and *negative* ω_c at which $\mathrm{Re}q=1$. ω_c is given explicitly for small γ as

$$\omega_c\to\tfrac{1}{27}(\tfrac{1}{2}\gamma\pi^2)^{-2}\ \text{ as }\gamma\to 0$$

which equals -1.52×10^3 at $\gamma=0.001$ and -60.84 at $\gamma=0.005$.

How does this compare with the real spectrum seen in our numerical computation? At any finite $s_{\max}$, we do not get an absolute cutoff of the spectrum at $\mathrm{Re}q=1$. Instead, some amount of exponential growth is tolerated at any fixed $s_{\max}$; this gives rise to an observed $\omega_c(s_{\max})$. For example, at $\gamma=0.005$ symmetric we have $\omega_c(4)=-8.91$ and $\omega_c(6)=-18.8$, corresponding to $\mathrm{Re}q$ of 1.94 and 1.49, respectively. Clearly, we are not all that close to the $s_{\max}=\infty$ limit; aside from this, however, our description works well. The actual wave vector as can be measured from the eigenfunction reproduces the eigenvalue when substituted into the dispersion relation, and the spectrum does cut off at some $\mathrm{Re}q$, which approaches 1 (albeit slowly) as $s_{\max}\to\infty$. Finally, all these modes are strongly damped in time and are of no significance for the stability problem at hand.

The real part of the continuum is fundamentally different from the complex branch. For any $\mathrm{Im}\omega=0$, $\mathrm{Re}q\ge 0$, there are two modes corresponding to positive and negative imaginary q which satisfy the dispersion relation. This allowed us, in a manner discussed, for example, in the treatment of the local model of Ref. 11, to satisfy the boundary conditions at both the tip and infinity. This part of the spectrum can therefore be characterized completely analytically. For any complex ω, there is only one value of $\mathrm{Im}q$ for a given $\mathrm{Re}q$. The simultaneous requirement of satisfying all boundary conditions can only occur if $\mathrm{Re}\omega$ is picked to be a uniquely determined function of $\mathrm{Im}\omega$, a function that depends on the details of the nonasymptotic pieces of the stability operator. We can determine this dependence only numerically. Furthermore, the function can and does depend on whether the modes are symmetric or antisymmetric.

In Fig. 6(a) we plot the complex symmetric continuum at $s_{\max}=6$, $\gamma=0.005$, $N=300$. $\mathrm{Im}\omega$ increases, reaches a maximum, and then decreases until it hits zero at $\mathrm{Re}\omega=\omega_c$, the start of the real continuum. In Fig. 6(b) we have plotted the same data as $\mathrm{Re}q$ versus $\mathrm{Im}q$. Notice that the complex branch is generated by varying $\mathrm{Im}q$ from 0 to $\mathrm{Im}q_c$, the start of the real spectrum. Of course, the same statements regarding the ultimate irrelevance of the modes with $\mathrm{Re}q\ge 1$ apply to the complex modes as well as the real modes discussed above. As $s_{\max}\to\infty$, the two spectra will meet at $\mathrm{Re}q=1$.

From the point of view of the finger, the most important part of the spectrum is the region around $\mathrm{Im}q=0$. In particular, since the complex modes continue to satisfy the dispersion relation, we must know how $\mathrm{Re}q$ behaves so

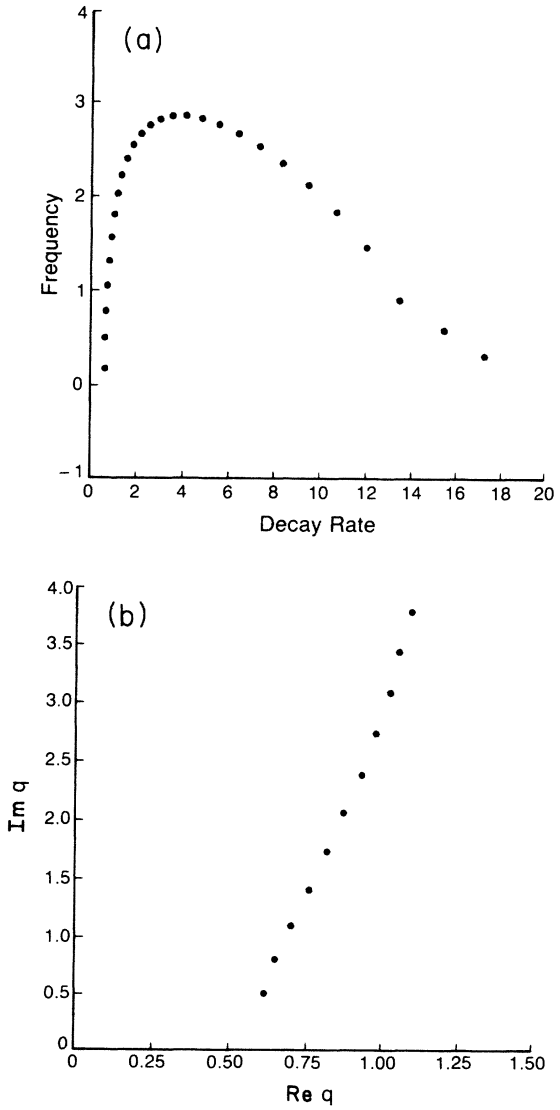

FIG. 6. Complex continuum at $s_{\max}=6$, $N=300$. (a) $\mathrm{Re}\omega$ vs $\mathrm{Im}\omega$. (b) $\mathrm{Re}q$ vs $\mathrm{Im}q$.

as to compute ω. If $\mathrm{Re}q=0$ at $\mathrm{Im}q=0$, the continuum would only be marginally stable. This is indeed what happens at exactly $\gamma=0$ for the symmetric operator, in the following sense. At $\gamma=0$, the finger solution exists for all λ and therefore there is a zero mode corresponding to changing λ. Since $\mathrm{Re}q$ is the growth rate of the normal displacement in the asymptotic far form tip region, changing the width asymptotically requires $\mathrm{Re}q=0$. Similarly, in *perturbation* theory at finite γ, such a mode must continue to exist. *Nonperturbatively,* we know that there is no such zero mode and that therefore the symmetric stability operator continuum must have a gap. That is, the spectrum should start at $\mathrm{Re}q>0$ and hence $\mathrm{Re}\omega<0$. This is what we would like to verify numerically.

In Fig. 7 we have plotted the bottoms of the symmetric and antisymmetric continua at $\gamma=0.005$, extrapolated to $s_{\max}=\infty$ using the ideas in Sec. V. Notice first the finite gap; $\mathrm{Re}\omega$ is always negative and the finger is stable. Likewise, in Fig. 8 we show the $\gamma=0.001$ symmetric continuum. The results are similar. In all cases we have checked, all $\mathrm{Re}\omega<0$ and there is no instability. Notice, however, the strange behavior of the bottom of the symmetric continuum. Whereas the antisymmetric modes nicely converge to a curve which cuts off at some negative value for $\mathrm{Re}\omega$, the last few modes of the symmetric continuum seem to be offset from the rest of the branch. We do not fully understand this behavior, although we feel that it may be connected with the widening mode discussed above. Some evidence for this can be obtained by plotting the eigenfunction as we have done in Fig. 9 and verifying that it is a pure exponential with $\mathrm{Im}q=0$.

It is in general quite hard to say much more about these modes. We would need to go to much larger $s_{\max}$ before we could be confident of any quantitative prediction. For example, it is possible that the anomalous behavior at small $\mathrm{Im}\omega$ is an artifact of our cutoff. Nevertheless, the sum total of all our runs at differing cutoffs and parameters indicate no sign of any instability. That is, the continuum consistently hits the $\mathrm{Im}q=0$ axis at finite and positive $\mathrm{Re}q$. In fact, we have never found a mode at any negative value of $\mathrm{Re}q$, either in the real or complex parts of the spectrum. Coupled with the results for the discrete modes presented in Sec. VI, we can safely conclude that at least for $\gamma\geq 0.0005$, $\lambda=\frac{1}{2}$ fingers are linearly stable. We will present additional data for $\lambda\neq\frac{1}{2}$ in paper II.

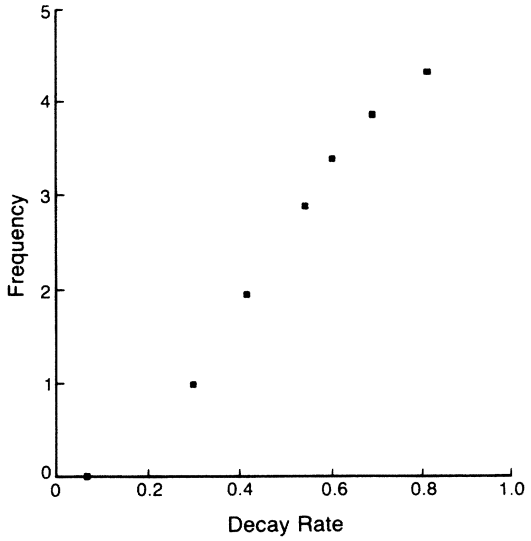

FIG. 8. Extrapolated complex continuum, symmetric only, at $\gamma=0.001$.

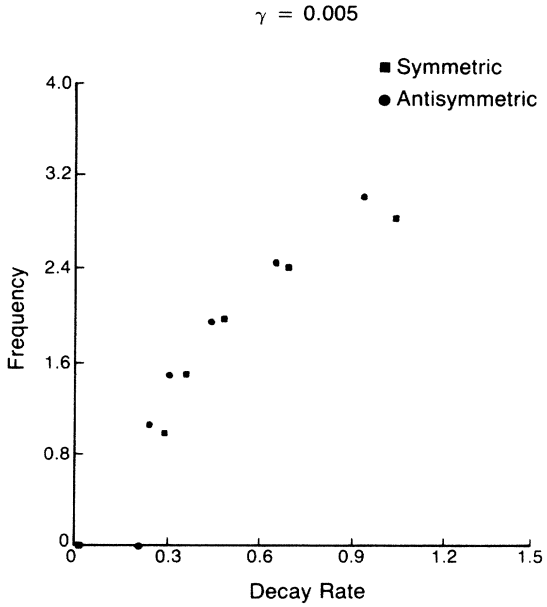

FIG. 7. Extrapolated complex continuum at $\gamma=0.005$, both symmetric and antisymmetric modes.

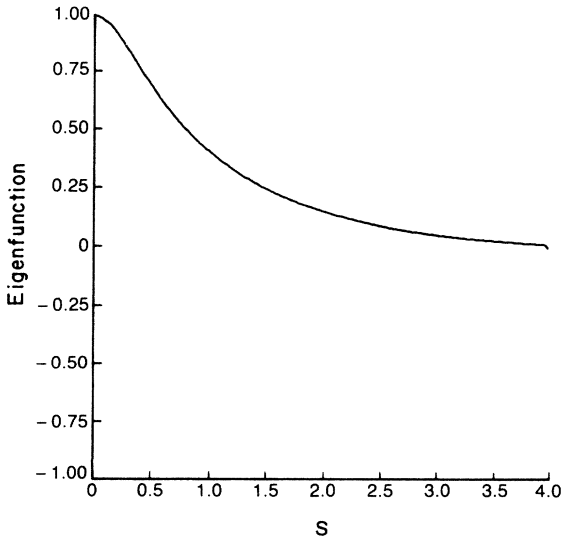

FIG. 9. Widening eigenfunction, bottom of the continuum at $\gamma=0.001$.

VIII. CONCLUSIONS

The purpose of this paper was to present an analytic and numerical framework which allows us to understand the spectrum of small oscillations around the Saffman-Taylor finger. The major results that we will need to carry over to the second paper of this series are the following.

(1) At any fixed λ, a steady-state shape and a resulting stability operator can be computed as a power series in γ, the surface tension. Although we have carried out this expansion to only one order, nothing in principle prevents us from proceeding further.

(2) The spectrum of the operator at *any* nonzero value of γ is drastically different from that at $\gamma=0$. This makes a careful numerical analysis crucial for demonstrating the stability of the finger solution.

(3) There is a large response of the spectrum to small noise in the computer algorithm. Specifically, at small γ, small noise can destabilize the steady-state solution.

(4) The continuum runs from $\mathrm{Re}q=0$ to $\mathrm{Re}q=1$, generating a real branch and a complex branch. These modes are always damped in time.

(5) There are both symmetric and antisymmetric discrete modes which at $\lambda=\frac{1}{2}$ with no noise seem to be stable to very low γ. We conjecture that they will remain stable all the way to $\gamma=0$.

(6) There is an approximate zero mode which is not at exactly $\mathrm{Re}\omega=0$ for any finite γ. Somewhat surprisingly, this mode does not seem to approach zero as γ is decreased.

In the following paper, we generalize our calculation to $\lambda\neq\frac{1}{2}$ and relate the stability properties to the selection of finger width. This will allow us to present a complete picture of the Saffman-Taylor finger, at least from a phenomenological point of view.

ACKNOWLEDGMENTS

We would like to acknowledge useful discussions with Len Schwartz and D. Bensimon, both of whom shared many of their results with us prior to publication. We would also like to acknowledge useful remarks by R. Dashen, L. Kadanoff, A. Libchaber, and H. Neuberger.

APPENDIX

In this appendix we present without derivation the formulas derived in Secs. II–IV generalized to arbitrary λ.

First, the generalization of the shape correction is

$$\delta_0(\psi)=\frac{2\gamma\lambda}{D}\{\lambda[1+\cos(\pi\psi)]\kappa^{(0)} -(1-\lambda)\sin(\pi\psi)T(\kappa^{(0)})\}\ , \tag{A1}$$

where

$$D=4\{(1-\lambda)^2+[\lambda^2-(1-\lambda)^2]\cos^2(\pi\psi/2)\}$$

and the curvature of the Saffman-Taylor solution is given by

$$\kappa^{(0)}=\frac{\frac{1}{2}\pi\lambda(1-\lambda)\cos(\pi\psi/2)}{D/4}\ . \tag{A2}$$

Explicitly performing the evaluation of the integral operator $T(\kappa^{(0)})$, we arrive at the expression

$$\frac{2\gamma\lambda}{D}\left\{\lambda[1+\cos(\pi\psi)]\kappa^{(0)}-(1-\lambda)\sin(\pi\psi)\left[\frac{2(1-2\lambda)}{\lambda D}\sin(\pi\psi)+\frac{4\lambda(1-\lambda)\cos\left[\frac{\pi\psi}{2}\right]}{D^{3/2}}\ln\left[\frac{1+\frac{2(1-\lambda)}{\sqrt{D}}\sin\left[\frac{\pi\psi}{2}\right]}{1-\frac{2(1-\lambda)}{\sqrt{D}}\sin\left[\frac{\pi\psi}{2}\right]}\right]\right]\right\}\ . \tag{A3}$$

The stability operator was given in the text as Eq. (15). The left-hand side becomes, for general λ,

$$\dot{\delta}\left[\frac{D+4\pi\lambda(1-\lambda)\delta_0}{4\cos^2(\pi\psi/2)}\right]+\left[\frac{1-\lambda}{\lambda}\right]\left[\tan\left[\frac{\pi\psi}{2}\right]\delta\right]'\ . \tag{A4}$$

The terms on the right-hand side become

$$\tfrac{1}{2}\int_{-1}^{1}d\psi'\cot[\tfrac{1}{2}\pi(\psi-\psi')]\{(\delta-\gamma\kappa^1[\delta])'(\psi')\}\ , \tag{A5a}$$

with

$$\kappa^1[\delta]=\frac{-2\delta''\cos(\pi\psi/2)}{\sqrt{D}}\ \frac{-4\pi(1-\lambda)^2\sin(\pi\psi/2)}{D^{3/2}}\delta'-\pi^2\delta\left[\frac{2\lambda^2(1-\lambda)^2\cos(\pi\psi/2)}{D^{5/2}}-\frac{2(1-\lambda)^2\cos(\pi\psi)}{D^{3/2}\cos(\pi\psi/2)}\right]$$

and

$$\tfrac{1}{2}\int d\psi'\cot\left[\frac{\pi}{2}(\psi-\psi')\right]\left[\left[\delta\frac{\partial}{\partial\psi'}[\delta_0\tan(\pi\psi'/2)]'\right]'+\{[l'(\psi)-l'(\psi')]\delta'(\psi')\}+\{[l(\psi)-l(\psi')]\delta''(\psi')\}\right] \tag{A5b}$$

with

$$l(\psi)=\frac{1-\lambda}{\lambda}\tan\left[\frac{\pi\psi}{2}\right]\delta_0+\gamma T[\kappa^{(0)}]\ ,$$

which can be explicitly evaluated as before, and finally

$$+\frac{\partial}{\partial\psi}[\delta(\delta_0-\gamma\kappa^{(0)})']\ . \tag{A5c}$$

[1]D. Kessler and H. Levine, Phys. Rev. A **32**, 1930 (1985).

[2]D. Bensimon, Phys. Rev. A **33**, 1302 (1986).

[3]A. J. Degregoria and L. Schwartz (unpublished).

[4]H. J. S. Hele Shaw, Nature (London) **58**, 34 (1898).

[5]See, for example, A Sheidigger, *Physics of Flow Through Porous Media* (University of Toronto Press, Toronto, 1974).

[6]P. G. Saffman and G. I. Taylor, Proc. R. Soc. London Ser. A **245**, 312 (1958).

[7]R. A. Wooding, J. Fluid Mech. **37**, 477 (1967); E. Pitts, *ibid.* **97**, 53 (1980).

[8]The approach to a single finger may be quite lengthy for fluids of similar viscosity. See J. Maher, Phys. Rev. Lett. **54**, 1498 (1985), and G. Trygvasson and H. Aref, J. Fluid Mech. **136**, 1 (1983).

[9]C. W. Park and G. M. Homsy, Phys. Fluids **28**, 1583 (1985); A. Libchaber and P. Tabeling (unpublished); E. Ben-Jacob (unpublished); J. Nittman, G. Daccord, and H. E. Stanley, Nature (London) **314**, 141 (1985).

[10]For a review of early theoretical work on dendritic growth, see J. S. Langer, Rev. Mod. Phys. **52**, 1 (1980).

[11]For some recent theoretical developments, see R. C. Brower, D. Kessler, J. Koplik, and H. Levine, in Proceedings of the 5th Conference on Physico-Chemical Hydrodynamics, 1984 (unpublished), and references therein.

[12]G. P. Ivantsov, Dokl. Akad. Nauk SSSR **58**, 567 (1947).

[13]For a review of experimental work, see M. Glicksman, Mater. Sci. Eng. **65**, 45 (1984), and references therein.

[14]J. W. McLean and P. G. Saffman, J. Fluid Mech. **102**, 455 (1981).

[15]J. M. Vanden-Broeck, Phys. Fluids **26**, 2033 (1983).

[16]See Trygvasson and Aref, Ref. 8; Degregoria and Schwartz, Ref. 3; and Libchaber and Tabeling, Ref. 9.

[17]The relationship between this stability operator and the true stability operator around the steady-state solution will be discussed at length in the following paper.

[18]D. Kessler, J. Koplik, and H. Levine (unpublished).

[19]J. W. McLean, Ph.D. thesis, California Institute of Technology 1980.

[20]H. Müller-Krumbhaar and J. S. Langer, Acta Metall. **29**, 145 (1981).

[21]D. Kessler and H. Levine (unpublished).